TESLA Report 2004-07

Beam Power Limitations during the TTF2 Injector Commissioning

V. Balandin, K. Flöttmann, and N. Golubeva
DESY, Hamburg

Contents

1 Introduction

For commissioning of an injector of the TESLA Test Facility Phase 2 (TTF2) the particles generated on the cathode are not supposed to go through the entire linac, but the part of the beam pipe ($\sim 0.576\,m$ long) in the front of the ACC2 module is removed, and the vacuum is closed by the exit window followed by a temporary beam dump [1]. The $1\,mm$ thick exit window made of stainless steel is placed at the distance of 36.747 m, as measured from the cathode position, and the dump is just a copper block with dimensions of $11.9 \times 12.5 \times 15.2\ cm^3$ ($W \times H \times L$).

To avoid a break of the vacuum system in the considered layout, the number of particles, penetrating through the window per unit area per unit time, should not exceed some safety limits defined by the window material properties and design.

Because the exit window is already manufactured (it was foreseen for the accelerating module dark current measurements and is a vacuum flange [2]), in this note we will only address questions connected with the estimation of operational parameters (bunch charge, number of bunches in the train, beam spot area at the window location) which this window may withstand without being damaged.

Note, that the most critical point is the theoretical prediction of the beam spot area at the window location. Many parameters can be involved, including the charge and emittance coming from the cathode, the energy gain in the ACC1 accelerating module, and the optics settings. Attempting to give recommendations which will minimize the consequences of possible operational mistakes, we present result of our estimation of the maximal allowed number of bunches in the train as a function of the rms beam spot area. So, at first, the information about the beam spot area should be obtained in a single bunch operation, and only then, having the estimation of allowed number of bunches, one can switch to multibunch mode.

Nevertheless, being useful, such estimations tell us nothing about the beam spot area which one should expect, or what can be done in order to enlarge it. It is a question of an optics setting. So, we look also for the beam optics, which maximizes the beta functions at the exit window location, taking into account different operational regimes (bunch compressor BC2 is switched on or off, FODO structure is set or not set, and so on). Note, that the optics used is the theoretical optics taken from [3]. It starts from the quadrupole doublet of the ACC1 module and uses as initial values (as a first

guess) the Twiss parameters suggested in [4] on the basis of the numerical simulations of the beam dynamics in the upstream part of the linac. The question how to bring the real beam behaviour in the correspondence to these optics is beyond the purpose of this note and is not considered.

2 Operational Modes and Beam Optics

Following [1], we consider three main variants of the operations during injector commissioning. The corresponding parameters are listed in table 1 and the short description of each mode one can find below.

- **Nominal operational mode.**

  The optics is the same which is currently proposed to be used in the further TTF2 operation. The only difference is that the allowed beam intensity is lower to ensure the survival of the temporary exit window.

- **Commissioning operational mode.**

  This mode is, in main, a step towards establishing the nominal operation mode under relaxed limitations on the possible beam intensity, that can be achieved by tuning last three quadrupoles in DBC2 to enlarge the beta functions at the window location (see following subsection for details).

- **High current operational mode.**

  The optics is proposed for tests and measurements: for high current operations, high gradient tests [5], quadrupole scan for measuring emittance.

2.1 Beam Line Used for Optics Tuning

Here we describe briefly the part of the TTF2 linac [6], [7] which we will use for the optics tuning. It includes the quadrupole doublet of the ACC1 module (two superconducting quadrupoles), a temporary beam line ($\sim 5\,m$, place reserved for the third harmonic cavity), a quadrupole triplet, a first bunch compressor (which is called BC2 due to historical reasons), and a diagnostic section DBC2 followed by the exit window.

Table 1: Operational parameters.

Mode	Nominal	Commissioning	High current		Units
Energy	130	130	130	E_0	MeV
Bunch charge	1	1	1 and more	Q_b	nC
Emittance	1.5	1.5	1.5 - 10	ε_n	$mm \cdot mrad$
Bunch spacing	1	1	1	f_b	MHz
Repetition rate	10	10	1 - 10	f_t	Hz

Section DBC2 consists of three parts: a first matching section (five quadrupoles), a FODO lattice (7 quadrupoles with a single power supply, so that one can not tune them independently), and a second matching section (three quadrupoles). The FODO lattice is supposed to be used for emittance and beta functions measurements [6], [8]. Throughout this note only two options for the FODO lattice are considered, either the FODO structure is set with a phase advance of 45° per cell (in respect with its own periodic Twiss functions) or all quadrupoles of FODO lattice are switched off.

Both possibilities, the bunch compressor is switched on or off will be tested during the commissioning, and below we will refer to them as the BC2 operational regime[1] and as the SBC2 operational regime, respectively. At the changing of the operation between BC2 and SBC2 regimes the re-matching of the optics to the periodic beta functions of the FODO lattice has to be done to keep required conditions for beam parameters measurements. One has to compensate the differences in the path length and in the focusing properties (focusing of dipoles).

If one wants to measure the beam parameters using the FODO lattice, then its Twiss functions are fixed and thus only three downstream

[1] An angle of 18° is used for the bunch compressor BC2 [9].

quadrupoles (second matching section of DBC2) are available for the enlarging of theoretical beta functions at the window location. If FODO lattice can be switched off, one gets more flexibility, and that is an important option for the high current tests.

2.2 Possible Solutions for Optical Functions

The strategy chosen for selection of optical functions among many possible variants can be shortly described as follows.

- As the first step we concentrated on the nominal beam optics with bunch compressor BC2 switched on, i.e. on the optics which could be used for further TTF2 operations. When the solution which "looks good enough" and simultaneously satisfies all currently available beam dynamical constraints was found, we fixed it for all further considerations [3]. Of course, it can be changed and, probably, even will require some modifications with the experience gained from the actual commissioning.

- Considering another operational modes, we tried to satisfy their particular requirements staying as close to the nominal beam optics as possible, that looks quite reasonable, especially for commissioning purposes.

2.2.1 Nominal Beam Optics

The nominal optics has to match the upstream and downstream beam behaviour; has to preserve the periodic Twiss functions of the FODO structure; and, in the BC2 regime, has to organize the special optical functions in the bunch compressor region for preventing emittance growth due to coherent synchrotron radiation [10], [11].

Figures 1 and 2 show the behaviour of the chosen optical functions and the rms beam sizes for the BC2 and SBC2 regimes, respectively.

2.2.2 Commissioning Beam Optic

As it was already mentioned above, the commissioning optics differs from the nominal optics only by the setting of the last three quadrupoles. This

allows us to enlarge the beta functions at the exit window location by a factor of ~ 10 (see figure 3).

2.2.3 High Current Beam Optics

For high current operations the beam magnification achieved in the commissioning optics could be not sufficient. As a possible solution we propose simply to switch off all quadrupoles of DBC2 section (the setting of other quadrupoles remains the same as in the nominal optics). It increases the beta functions at the window by a factor of ~ 30.

Figures 4 and 5 show the behaviour of beta functions and rms beam sizes for the BC2 and SBC2 regimes, respectively.

Note, that on the basis of the high current optics (by switching on and tuning appropriately quadrupoles of the first matching section of DBC2) the optics suitable for making the quadrupole scan for emittance measurements is also possible.

3 Window Thermal and Mechanical Reaction to Beam Pulses

Penetrating through the window an electron deposits its energy as heat in the window material. The passage of a bunch of electrons creates an instantaneous temperature rise, because the bunch duration is essentially shorter than the characteristic thermal diffusion time for the stainless steel. Nonuniform rapid heating, confined to an area comparable with the beam spot size, creates local thermal stresses in the window and hence reduces its mechanical stability. If thermal stresses will exceed the stress limits, then micro-fractures can develop and even the window can fail completely.

In general, the analysis of effects, induced by high energy particles in matter, is very complicated problem and involves too many unknowns and different physical processes. Thus, to estimate the operational parameters which the exit window may withstand without being damaged, the choice of reasonable approximation plays a crucial role. We will follow to somewhat typical for accelerator physics approach, which is relatively simple, but usually gives reasonable results by introducing a safety margin (see, for example, [12], [13], [14], [15] and references therein).

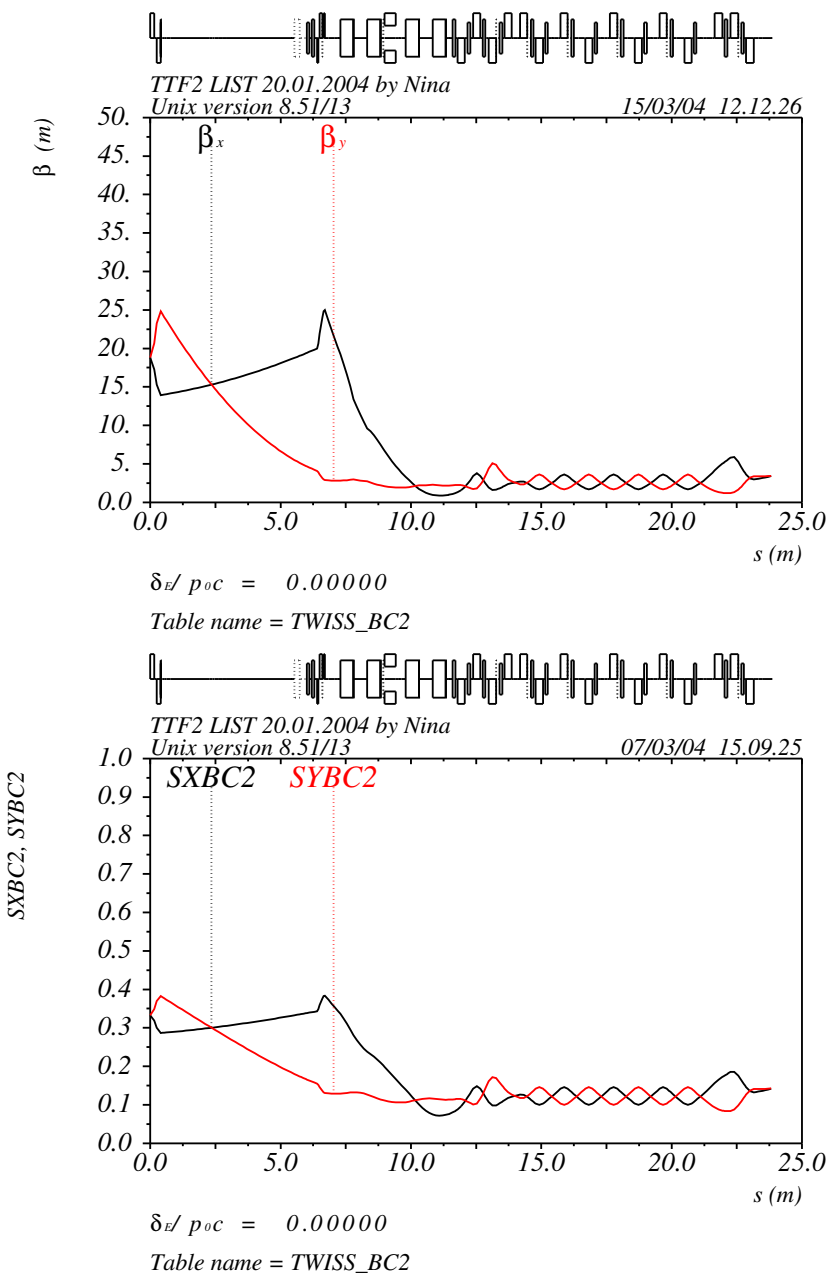

Figure 1: **Nominal optics.** Optical functions (top) and rms beam sizes in mm (bottom) for the BC2 regime. The energy is 130 MeV and $\varepsilon_{nx,ny} = 1.5\,mm \cdot mrad$.

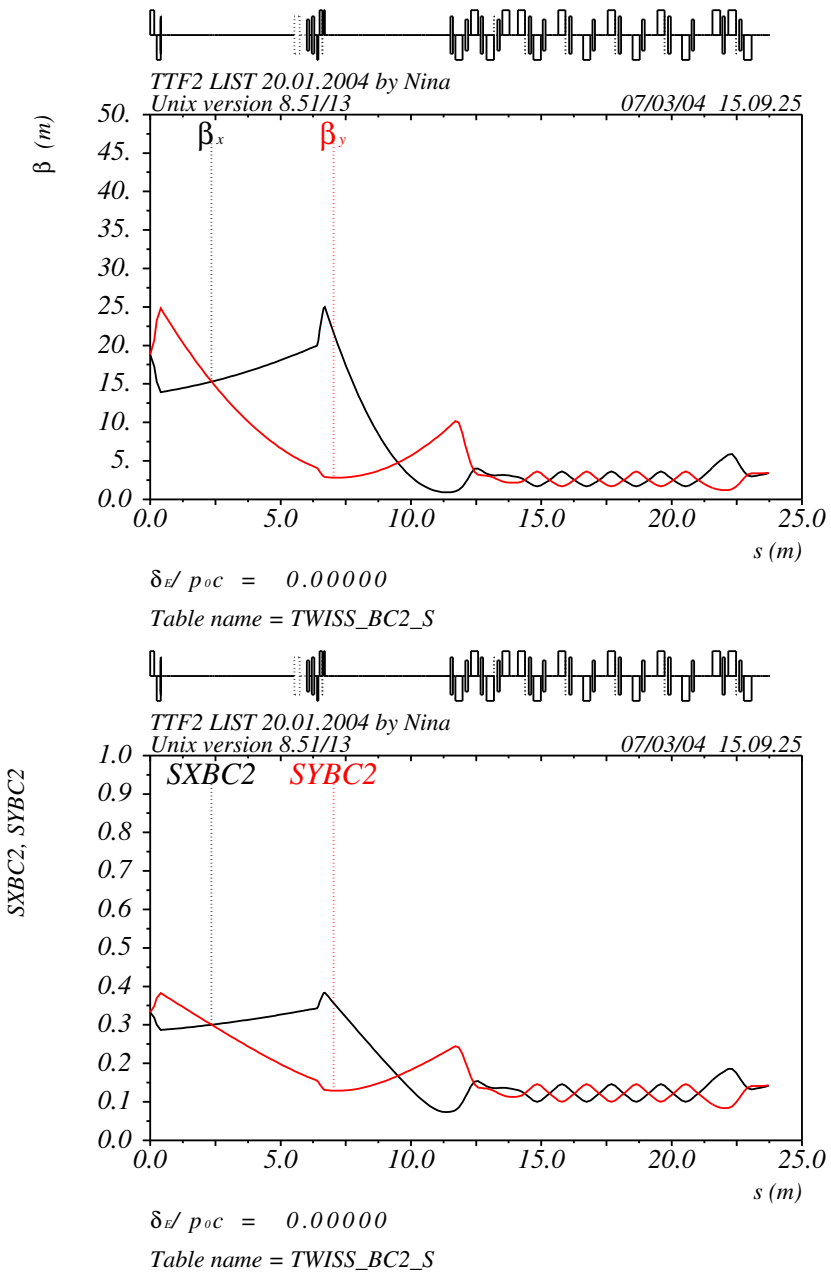

Figure 2: **Nominal optics.** Optical functions (top) and rms beam sizes in mm (bottom) for the SBC2 regime. The energy is 130 MeV and $\varepsilon_{nx,ny} = 1.5\,mm \cdot mrad$.

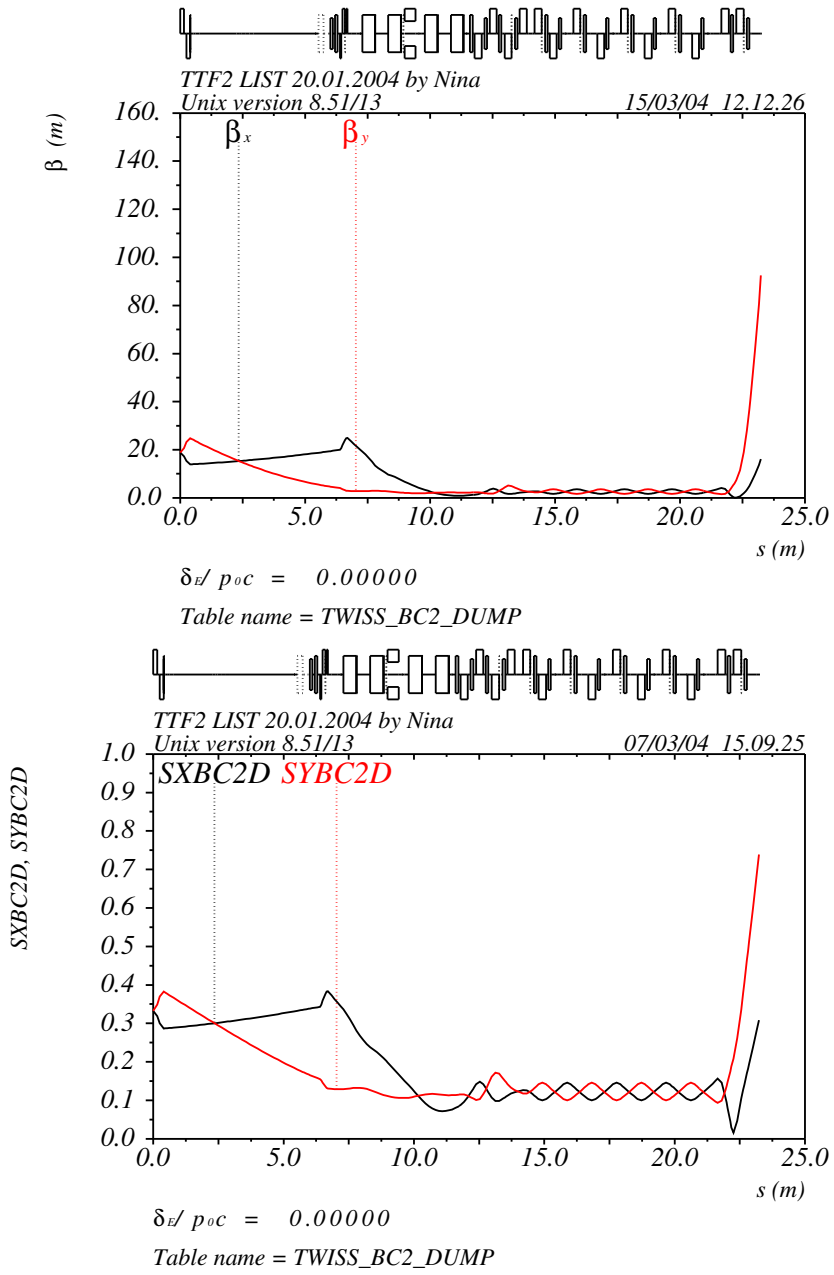

Figure 3: **Commissioning optics.** Optical functions (top) and rms beam sizes in mm (bottom) for the BC2 regime. The energy is 130 MeV and $\varepsilon_{nx,ny} = 1.5\,mm \cdot mrad$.

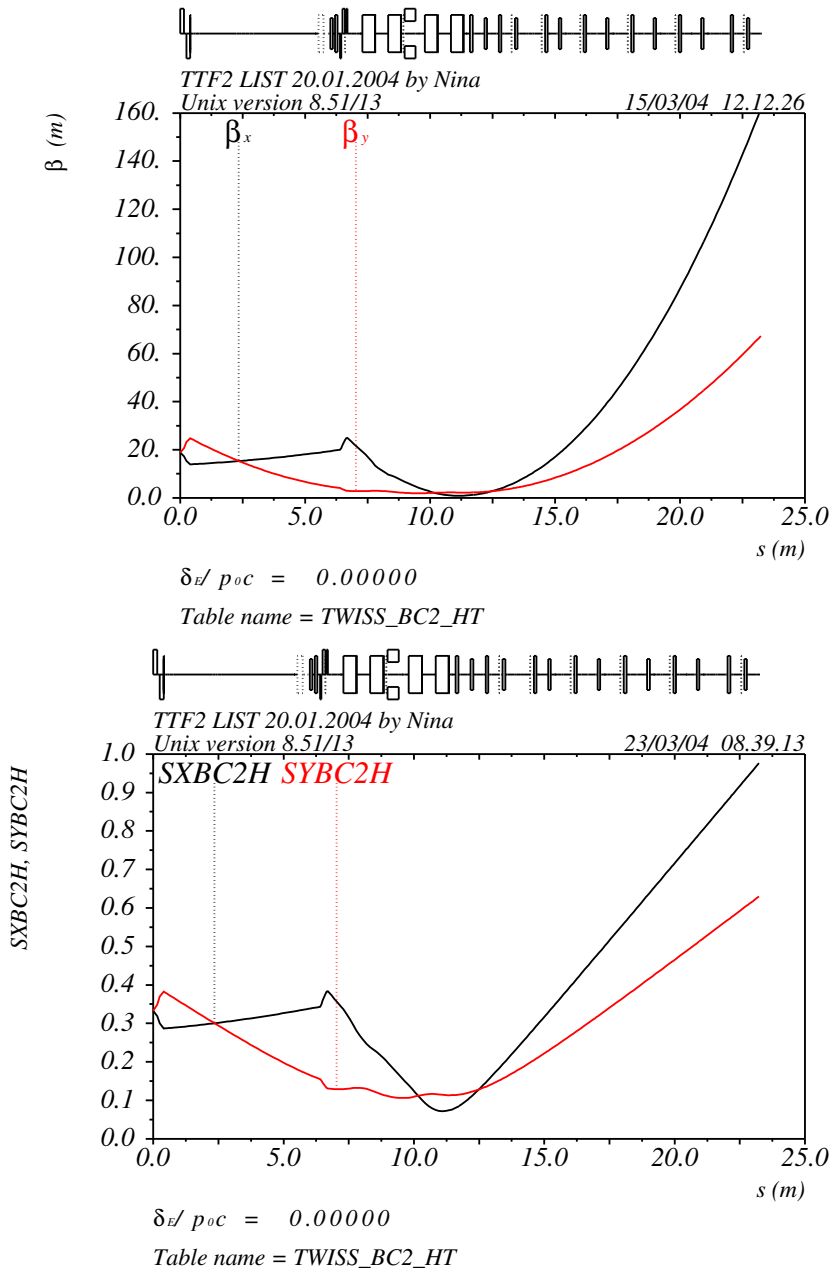

Figure 4: **High current optics.** Optical functions (top) and rms beam sizes in mm (bottom) for the BC2 regime. The energy is 130 MeV and $\varepsilon_{nx,ny} = 1.5\,mm \cdot mrad$.

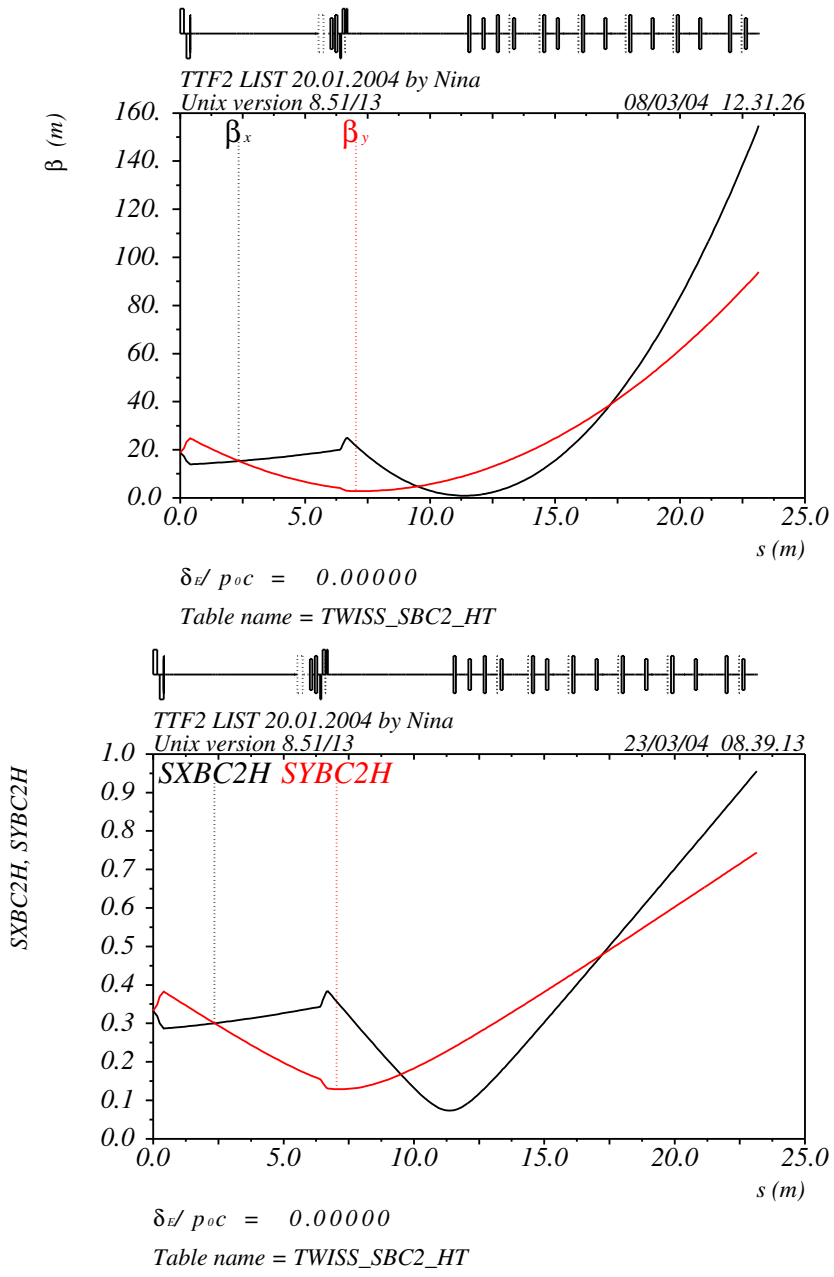

Figure 5: **High current optics.** Optical functions (top) and rms beam sizes in mm (bottom) for the SBC2 regime. The energy is 130 MeV and $\varepsilon_{nx,ny} = 1.5\,mm \cdot mrad$.

3.1 Properties of Window Material

The exit window is made from the stainless steel 316LN, and its central plate has $1\,mm$ thickness and diameter of $64\,mm$ [2]. The mechanical properties of the 316LN steel, which we will use through this note, were taken from [16]:

Density (g/cm^3)	8.0	$25°C$	ρ
Elastic Modulus (GPa)	196	$25°C$	E_y
Tensile Strength (MPa)	515		σ_{UTS}
Yield Strength (MPa)	205		$\sigma_{0.2}$
Endurance Limit (MPa)	240		σ_E
Specific Heat (J/g-K)	0.5	$0-100°C$	c_p
Thermal Expansion ($10^{-6}/°$)	16.0	$0-100°C$	α
Thermal Conductivity (W/cm-K)	0.162		λ

(1)

3.2 Rapid Energy Deposition and Resultant Temperature Rise

As it was already mentioned, we assume that the energy deposited during the bunch passage results in instantaneous temperature jump ΔT_{bc}. This temperature rise can be calculated by solving the following widely used equation

$$\frac{dE}{dm} = \int_{T_{in}}^{T_{in}+\Delta T_{bc}} c_p(T)\,dT\,, \tag{2}$$

where T_{in} is the initial temperature, dE/dm is the energy deposition density, and c_p is the specific heat (see, for example [17]).

Because the specific heat c_p stays nearly constant in the interesting for us temperature range (see table 1), the equation (2) can be simplified to the explicit formula

$$\Delta T_{bc}(x,y,z) = \frac{1}{c_p}\,\frac{dE}{dm}(x,y,z)\,. \tag{3}$$

3.2.1 Energy Deposition Density

When high energy electrons penetrate a thin slab of material, the electromagnetic cascade shower is practically not developed, and the main contribution to the energy deposition density comes from the ionization and excitation

of the atoms of the medium. Therefore the energy deposition density can be estimated analytically using the Bethe-Bloch formula, which predicts that dE/dm stays nearly constant over the slab thickness and relatively weakly (logarithmically) depends on the incoming particle energy.

Though the estimates given by the Bethe-Bloch formula are reasonably accurate, we used the more refined technique, and the interaction of a bunch with the exit window was investigated using the EGS4 (Electron-Gamma-Shower) software package for fast Monte Carlo simulations of the coupled electron-photon transport [18], [19]. Figure 6 shows a simulation example, the energy deposition density dE/dm in the stainless steel block from a single 130 MeV electron bunch as a function of longitudinal position. One sees, as it was expected, that the dE/dm is practically constant along the window thickness ($1\,mm$), and thus the difference

$$\frac{dE}{dm}(x,y,z) \; - \; \frac{1}{d}\int\limits_0^d \frac{dE}{dm}(x,y,z)\,dz \tag{4}$$

can be considered as negligible. Here d is the window thickness, and z and x, y are the longitudinal and transverse coordinates, respectively.

It motivates us to neglect also z-variation of the temperature field and in the following to study the time evolution only for the longitudinally average temperature[2]

$$\bar{T}(x,y,t) \; = \; \frac{1}{d}\int\limits_0^d T(x,y,z,t)\,dz \tag{5}$$

with the initial rise given now by

$$\Delta\bar{T}_{bc}(x,y) \; = \; \frac{1}{c_p}\left(\frac{1}{d}\int\limits_0^d \frac{dE}{dm}(x,y,z)\,dz\right) . \tag{6}$$

Moreover, we will often assume that the transverse profile of the energy deposition density follows the shape of incident electron beam. For example,

[2]Generally speaking, the difference between T and its longitudinally average $\bar{T}$ can become large due to boundary conditions on the outer and inner window surfaces. But as we will see below, for our particular situation the effect of these boundary conditions can be neglected with high precision.

if this shape is a Gaussian with covariance matrix

$$\Sigma \;=\; \begin{pmatrix} \sigma_{xx} & \sigma_{xy} \\ \sigma_{xy} & \sigma_{yy} \end{pmatrix} \equiv \begin{pmatrix} < x^2 > & < xy > \\ < xy > & < y^2 > \end{pmatrix} \tag{7}$$

and the beam energy spread is small (compared to mean energy), than instead of (6) we will use the formula

$$\Delta\bar{T}_{bc} \;=\; \frac{N_e}{2\pi\rho c_p a_{rms}} \left(\frac{1}{d} \int\limits_0^d \frac{dE}{dz}(\tau)\, d\tau \right) \exp\left(-\frac{1}{2} \Sigma^{-1} \begin{pmatrix} x \\ y \end{pmatrix} \cdot \begin{pmatrix} x \\ y \end{pmatrix} \right) , \tag{8}$$

where N_e is the number of electrons in the bunch, ρ is the material density, $a_{rms} \;=\; \sqrt{\det \Sigma}$ is the rms beam spot area, and dE/dz is the mean energy deposition by an electron per unit length along the beam axis.

3.2.2 Instantaneous Temperature Rise

With the 1 MHz spacing the cooling between bunches is so small[3], that the window heating can be considered as instantaneous even on the train passage time scale (up to $800\,\mu s$). In the case of Gaussian beam the maximal jump in temperature, which takes place near to the beam axis, can be estimated as

$$\Delta\bar{T}_{tr} \;=\; N_{bc} \cdot \Delta\bar{T}_{bc} \;=\; \frac{N_e \cdot N_{bc}}{2\pi\rho c_p a_{rms}} \cdot \left(\frac{1}{d} \int\limits_0^d \frac{dE}{dz}(\tau)\, d\tau \right) , \tag{9}$$

where N_{bc} is the number of bunches in the train.

3.3 Time Evolution of Window Temperature

3.3.1 Equation for Average Temperature

Energy can be released from both sides of the window central plate in the form of thermal radiation, and the outer side is, additionally, cooled by surrounding air, which leads to the following non-linear boundary conditions

$$\lambda \left. \frac{\partial T}{\partial z} \right|_{z=0} \;=\; \varepsilon\, \sigma\; T^4 \Big|_{z=0} , \tag{10}$$

[3]The cooling between bunches becomes visible only for the small beam spot areas. Neglection of this effect gives us an additional safety margin.

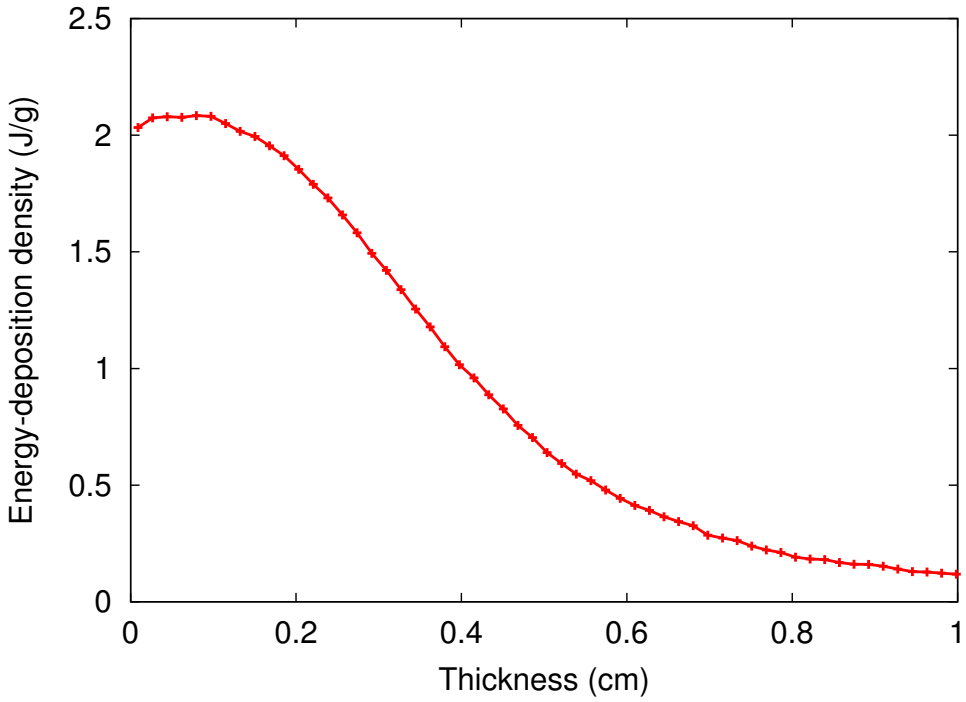

Figure 6: Energy-deposition density (close to beam axis) in the stainless steel block from a single bunch as a function of the longitudinal position. The bunch charge is 1 nC, the particle energy is 130 MeV, the shape of incident beam is a uncoupled Gaussian with $\sigma_x = \sigma_y = 0.1\,mm$.

$$-\lambda \left.\frac{\partial T}{\partial z}\right|_{z=d} = h\left(T|_{z=d} - T_{air}\right) + \varepsilon\,\sigma\,\left(\left.T^4\right|_{z=d} - T_{air}^4\right), \tag{11}$$

where σ is the Stefan-Boltzman constant, ε is the surface emissivity, T_{air} is the air temperature, and h is the convection heat transfer coefficient.

Integrating both sides of the three dimensional equation of heat diffusion

$$\rho\, c_p \frac{\partial T}{\partial t} = \nabla\,(\lambda\,\nabla\, T) + Q(x,\, y,\, z,\, t) \tag{12}$$

with respect to variable z, substituting boundary conditions (10) and (11) instead of z-derivatives, dividing both sides by d, and then neglecting terms proportional to $T - \bar{T}$, we obtain equation describing the evolution of the average temperature $\bar{T}$ in the window central plate

$$\rho\, c_p \frac{\partial \bar{T}}{\partial t} = \frac{\partial}{\partial x}\left(\lambda \frac{\partial \bar{T}}{\partial x}\right) + \frac{\partial}{\partial y}\left(\lambda \frac{\partial \bar{T}}{\partial y}\right) - \frac{h}{d}\left(\bar{T} - T_{air}\right)$$

$$- \frac{\varepsilon\,\sigma}{d}\left(\bar{T}^4 - T_{air}^4\right) - \frac{\varepsilon\,\sigma}{d}\,\bar{T}^4 + \bar{Q}(x,\, y,\, t)\,. \tag{13}$$

Here

$$\bar{Q}(x,\, y,\, t) = \frac{1}{d}\int\limits_0^d Q(x,\, y,\, z,\, t)\, dz \tag{14}$$

is the longitudinally averaged density of internal heat sources.

3.3.2 Dominant Cooling Mechanism

Besides the discussed above cooling mechanisms (10) and (11) the heat from the window central plate is transfered to the window flange by means of heat conduction. The flange volume is about 40 times larger than central plate volume, and taking additionally into account that flange is connected to another accelerator equipments, we can consider its temperature, T_{fl}, as independent on the central plate temperature. It gives us the boundary condition

$$\left.\bar{T}\right|_{x^2+y^2=R^2} = T_{fl}\,, \tag{15}$$

where R is the plate radius.

Numerical integration of the equation (13) with boundary condition (15) and initial condition

$$\bar{T}(x, y, 0) \;=\; T_{in} \tag{16}$$

has shown us, that in the intersting for us temperature range the contribution of thermal radiation is completely negligible, and the effect of air cooling, if it is not forced, is also very small. So the terms proportional to ε and h in the equation (13) can be omitted.

Figure 7 presents, as an example, the temperature behaviour in the plate centre during the passage of three trains. The upper (red) curve is the case with cooling only due to heat conduction. The middle (green) curve shows the contribution of thermal radiation and natural air cooling. For this curve $\varepsilon \;=\; 1$ (maximal possible value, i.e. the plate is considered as a black body) and $h \;=\; 5 \cdot 10^{-3}\, W/(cm^2 K)$ (that is somewhat typical value for the convection heat transfer coefficient, if the air flow is not forced). So, as one can see, additional effect of these cooling mechanisms, even for the initial temperature as high as $100°C$, is inessential. The forced air flow can make the colling better (look at lower (blue) curve, where $h \;=\; 40 \cdot 10^{-3}\, W/(cm^2 K)$), but considering that the exit window is temporary, it is not proposed.

3.3.3 Equilibrium Solution

To get a filling what temperatures the window can reach during operations, let us consider the case when the beam spot is a round Gaussian and heat load due to the train passages is uniformly distributed in time. This leads to the problem of finding the stationary solution of the equation (13) with boundary condition (15) and with the density of internal heat sources $\bar{Q}(r)$ given by

$$\bar{Q}(r) \;=\; \Delta\bar{T}_{tr}\, f_t\, \rho\, c_p \cdot \exp\left(-\frac{r^2}{2a_{rms}}\right) . \tag{17}$$

This solution can be expressed as follows

$$\bar{T}(r) \;=\; T_{fl} \;+\; \frac{1}{\lambda}\int\limits_r^R \frac{1}{\tau}\left(\int\limits_0^\tau \eta\bar{Q}(\eta)d\eta\right) d\tau\,, \tag{18}$$

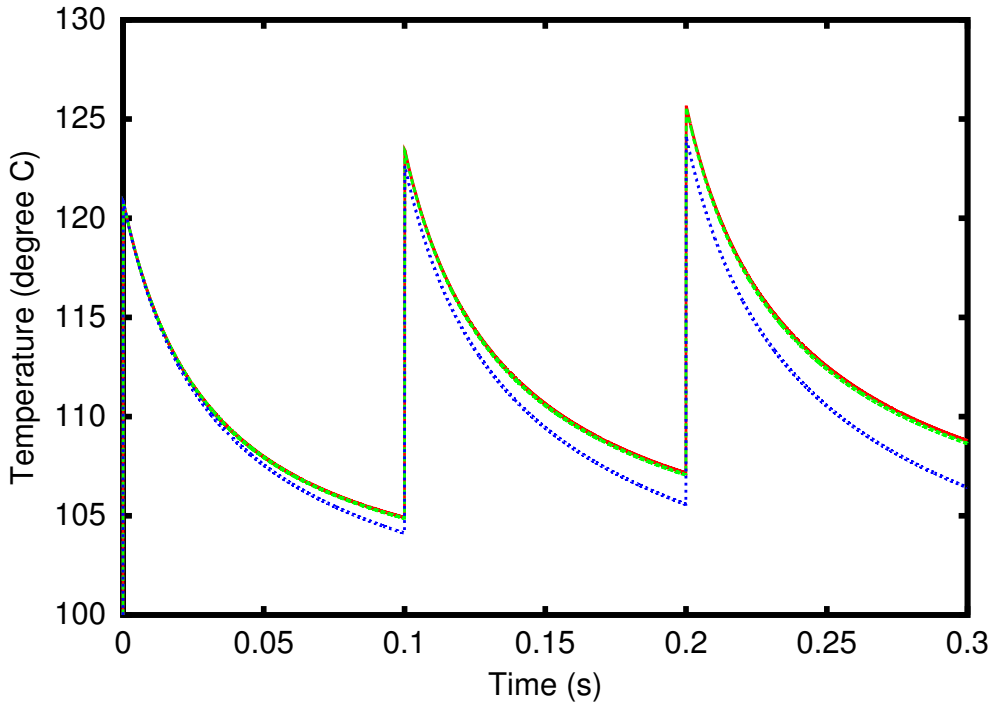

Figure 7: Temperature behaviour in the window plate centre. Initial temperature is $100°C$, $\sigma_x = \sigma_y = 0.5\,mm$, bunch charge is 1 nC, and train contains 100 bunches.

and one sees that the temperature decreases monotonically with radius and therefore the maximum value $\bar{T}_{max}$ is always reached in the centre of the window plate.

For the interesting for us case, when the plate radius is much larger than the beam radius one can obtain the approximate relation[4]

$$\bar{T}_{max} \approx T_{fl} + \left(\frac{1}{d}\int_0^d \frac{dE}{dz}(\tau)\,d\tau\right) \cdot \frac{N_e\,N_{bc}\,f_t}{4\pi\lambda} \cdot \ln\left(\frac{R^2}{2\,a_{rms}}\right). \qquad (19)$$

This formula can be used for the estimation of maximal number of bunches per train at which the maximal temperature of the window will stay below some predefined value during operations. Because the real temperature oscillates around the equilibrium, we add the oscillation amplitude (9) to the right side of (19) and obtain[5]

$$N_{bc} \leq \frac{2\pi(\bar{T}_{max} - T_{fl})}{N_e}\left(\left(\frac{1}{d}\int_0^d \frac{dE}{dz}(\tau)d\tau\right)\left(\frac{f_t}{2\lambda}\ln\left(\frac{R^2}{2a_{rms}}\right) + \frac{1}{\rho c_p a_{rms}}\right)\right)^{-1} \qquad (20)$$

As a result of the application of the formula (20), figure 8 shows the estimation of the maximal possible number of bunches per train as a function of the beam spot area with the assumption that the temperature $\bar{T}_{max}$ will not exceed $T_{fl} + 50°C$.

3.3.4 Time-Dependent Temperature Evolution

An accurate numerical integration of nonstationary problem was done with the aim to check the validity of analytical approximations given by (19) and (20). We considered the case of uniform in time heat load and the case when the window is heated only during the train passage. We used the different models of densities of internal heat sources, densities with Gaussian spatial shape and densities obtained as the results of shower simulation.

An example is shown in figure 9. For the parameters used the formula for stationary solution (19) gives the value of $\sim 70°C$, and the oscillation amplitude predicted by (9) is $\sim 20°C$, and it is about the same what one can see indeed.

[4]Note that the similar formula can be obtained for a non-Gaussian beam of a special shape as exact solution of the stationary problem (see, for example, [13]).

[5]Sometimes people use 0.5 or 0.75 of this oscillation amplitude.

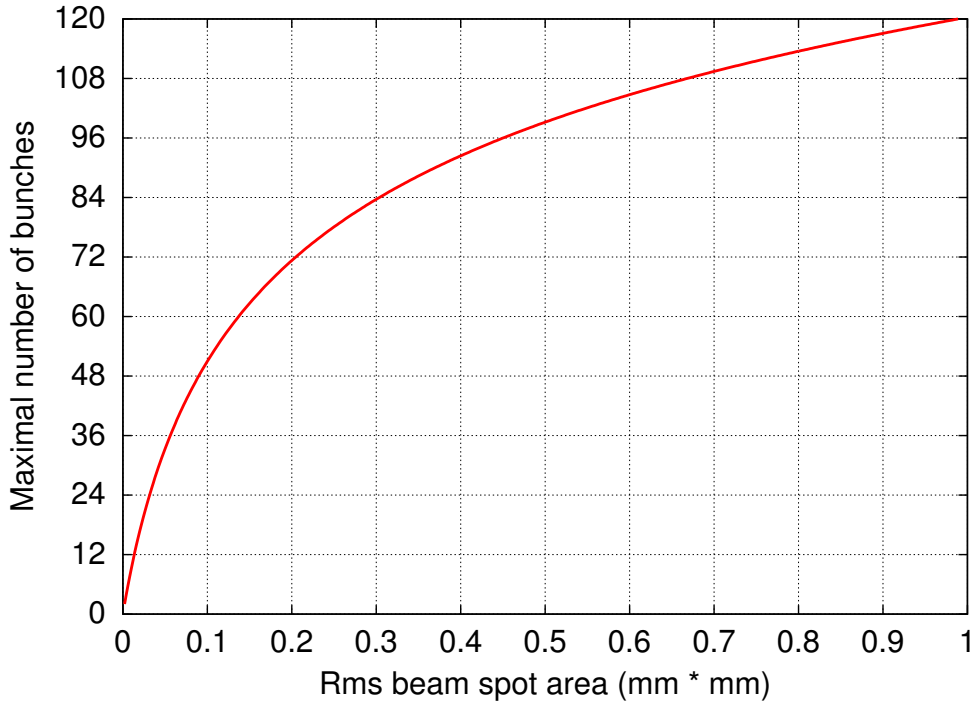

Figure 8: Maximal allowed number of bunches per train as a function of the beam spot area with the assumption that $\bar{T}_{max}$ will not exceed $T_{fl} + 50°C$. Repetition rate is 10 Hz.

Calculations with many different sets of parameters have indicated about the same level of coincidences. The only point which we would like to note is that the beams with round spots at the window location gives us the worst results among all other Gaussian beams with the same rms spot area a_{rms}. The worst in the sense that resulting maximal temperatures are higher and cooling time after the beam is switched off is longer.

3.4 Thermal Stresses and Mechanical Stability

The exit window separates the accelerator vacuum and the surrounding air, and hence, even without the beam impacts, experiences a stress due to air pressure. Assuming that a circular central plate of the window is fixed at the edge, this stress in the midpoint is given by

$$\sigma^{cen}_{static} \,=\, 0.49\,\frac{R^2}{d^2}\,p\,, \tag{21}$$

where $R \,=\, 32\,mm$ is the radius of the plate and $p \,\approx\, 0.1\,MPa$ (see, for example, [13]). At the edge the stress σ^{edg}_{static} is larger by a factor of about 1.5, and below we will use the average value

$$\sigma_{static} \,=\, \frac{\sigma^{cen}_{static} \,+\, \sigma^{edg}_{static}}{2}\,. \tag{22}$$

Additional load caused by the beam impacts will be estimated using an analytical formula for the central thermal stress in a radially constrained disk [20]

$$\sigma_{cyc} \,\simeq\, \frac{\alpha\,E_y\,\Delta\bar{T}_{tr}}{2}\,. \tag{23}$$

For safe operations the window must withstand not only an isolated load due to the combination of stresses (22) and (23), but must survive the regular thermal cycles[6], that reduces the safe stress limit.

For making the decision what operational parameters can be allowed, at first we will choose the working point in a Goodman diagram which will give us the allowed value for σ_{cyc}, then from (23) we will obtain the upper limit for the instantaneous temperature rise and, at the end, will connect this limit with beam parameters.

[6]The number of cycles during the commissioning can reach $\sim 10^7$ per month.

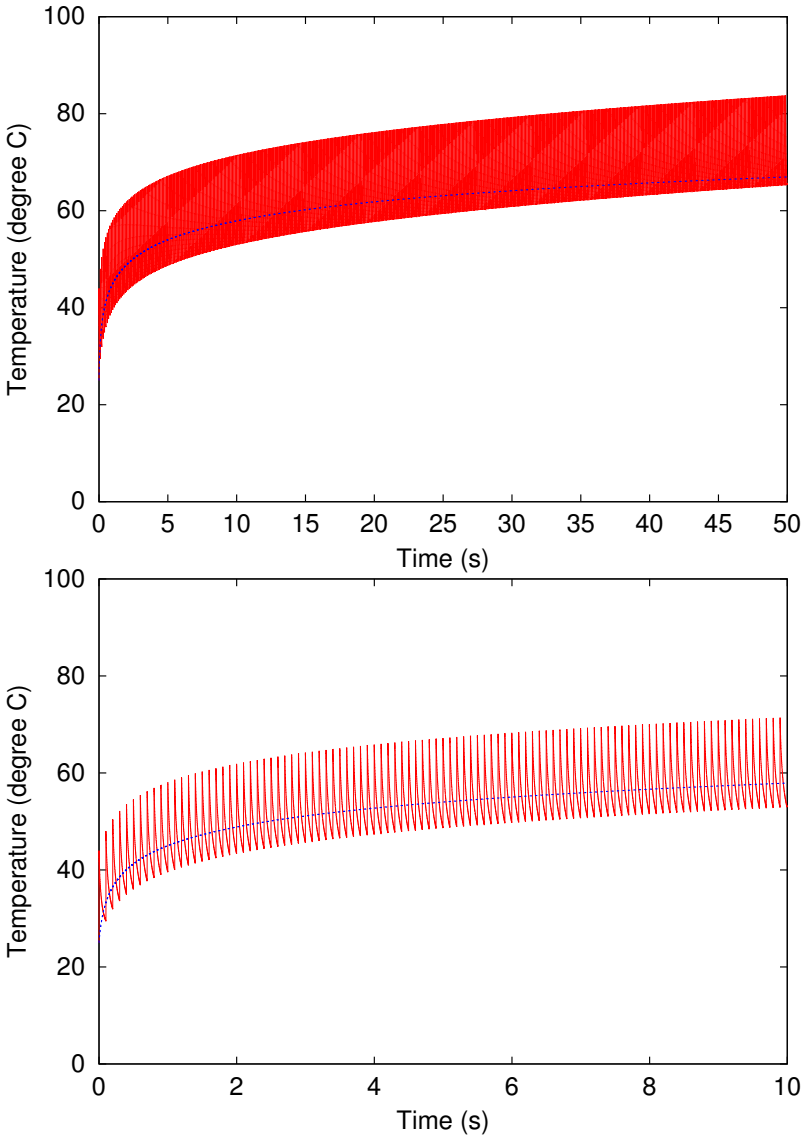

Figure 9: Transition of temperature in the beam centre from initial temperature $T_{in} = 25°$ to the steady-state oscillation for stainless steel window. The middle curve (blue) corresponds to the case of uniform in time heat load, and the oscillating curve (red) to the heating only during the train passage (100 bunches, 1 MHz bunch spacing, 10 Hz repetition rate). The rms beam spot area is $0.25\,mm^2$, the bunch charge is 1 nC. The lower figure is an enlarged part of the upper figure.

3.4.1 Goodman Diagram

The Goodman diagram, which we will use, is shown in figure 10 and represents graphically the so called 'Goodman criterion'. Its abscissa and ordinate are the mean stress σ_m and the alternating stress amplitude σ_a, which the material is subjected. The points Y and U marked on the horizontal axis are connected with single events. They are the yield stress (the stress necessary to cause a certain prescribed amount of plastic strain, usually 0.2%) and the ultimate tensile strength (the maximum stress that a material may withstand prior to fracture), respectively. The resistance to the thermal cycling is marked as the point E on the vertical axis. It is the endurance limit, i.e. the maximum stress that does not produce fatigue failure in a material for large number of cycles.

A straight line EU is known as the Goodman line. It separates safe and unsafe operating regimes (areas below and above this line). Because not only fracture, but already yielding may prevent the satisfactory operation, we show also the Soderberg line EY.

Let us assume that the thermal cycling load varies between zero and σ_{cyc} in time, and therefore the total load varies between σ_{static} and $(\sigma_{static} + \sigma_{cyc})$. Then the corresponding mean and alternating stress components are

$$\sigma_m \;=\; \sigma_{static} \;+\; \frac{\sigma_{cyc}}{2} \quad \text{and} \quad \sigma_a \;=\; \frac{\sigma_{cyc}}{2}\,. \tag{24}$$

Taking the numerical value of σ_{static} from (22) and considering σ_{cyc} as a variable parameter, we obtain the operating line SA (green), which consists of points with the coordinates $(\sigma_m,\ \sigma_a)$, and crosses the Goodman line EU at the point $A = (207.0\,MPa,\ 143.5\,MPa)$.

Now one has to choose the working point WP on the line segment SA. Usually a factor of safety is introduced in order to ensure the survival of the material. Since we do not know exactly how the stresses will vary in time, we use the safety factor sf, which is a value required to multiply the coordinates of the working point WP to cross the Goodman line:

$$(sf \cdot \sigma_m(WP),\ sf \cdot \sigma_{cyc}(WP)) \;\in\; EU\,.$$

The particular working point WP which we have chosen is also shown in figure 10. It has the safety factor of 4 with respect to the Goodman line and the safety factor of 2 with respect to the Soderberg line.

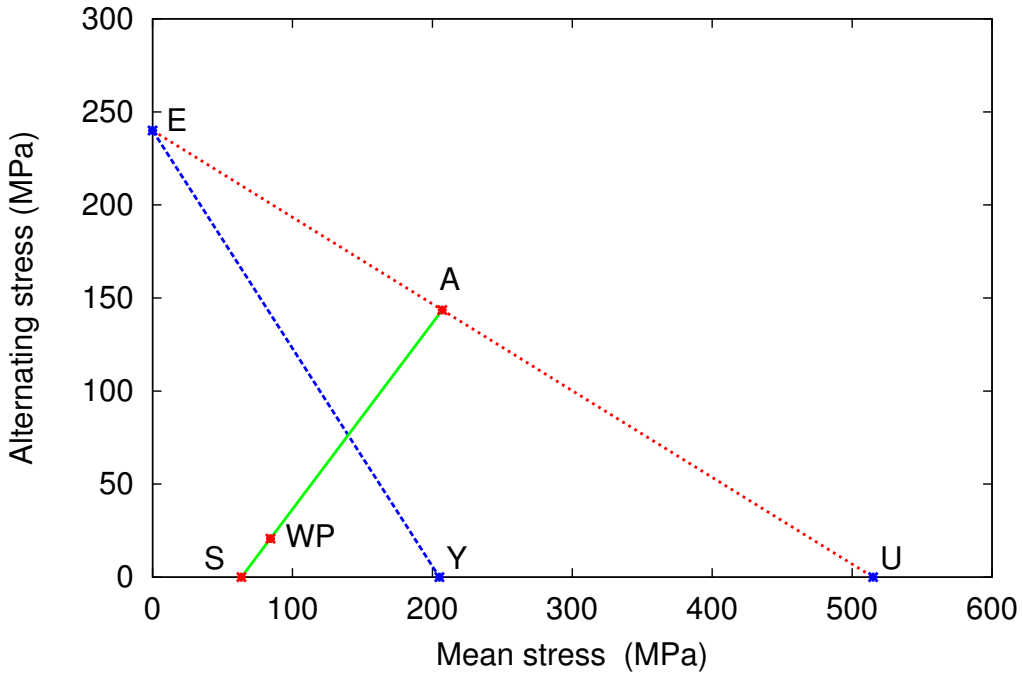

Figure 10: Goodman stress diagram for a 316LN stainless steel window.

The safety factor relates to many uncertainties of the material properties (material imperfections due to fabrication process and so on), to air pressure aspects, to the accuracy of the used analytical approach, and of course, to possible operational mistakes. It should be pointed out that, for our analysis, the mechanical and thermal properties of the stainless steel have been taken at the room temperature, and the reduction of the ultimate tensile strength and the endurance limit with the increasing of the temperature is also related to the chosen safety factor.

3.4.2 Beam Parameter Limitations

The value σ_{cyc} corresponding to the working point WP is $20\,MPa$. This number and (23) gives us the upper estimation of the maximal allowed temperature rise in the window material. And then using (9), we obtain the maximal number of bunches allowed per train as a function of the rms beam spot area, that is shown in figure 11.

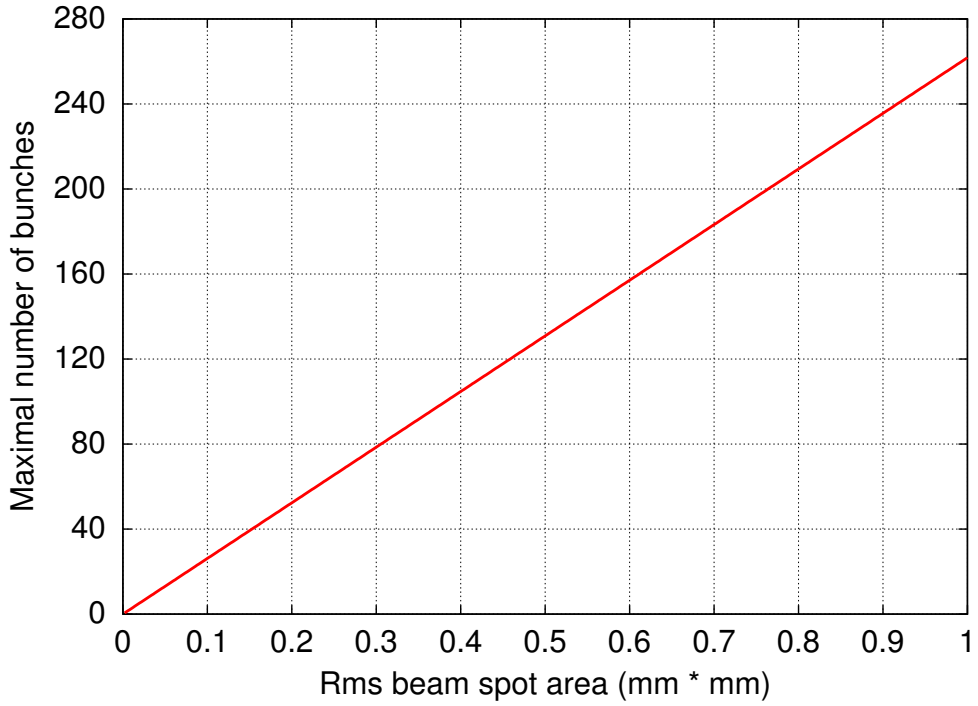

Figure 11: Maximal allowed number of bunches per train at which the instantaneous temperature rise corresponds to the working point WP, as a function of the rms beam spot area. Bunch charge - $1\,nC$. Particle energy - $130\,MeV$.

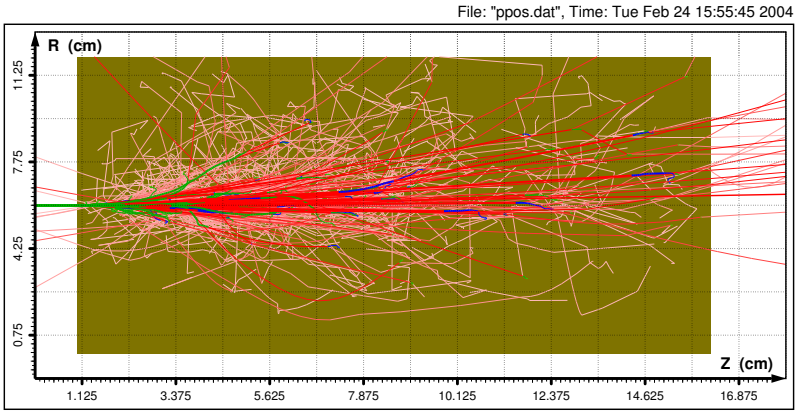

Figure 12: Shower development in the copper dump. Green curves - electrons, blue - positrons, and red - photons. Energy of input electrons is 130 MeV.

4 Temporary Beam Dump

The temporary beam dump is a copper block installed close to the exit window. At the parameters proposed for the commissioning (table 1) the average beam power which dump has to absorb is low, and hence an additional cooling except the natural air cooling does not seem to be needed.

The failure of the dump material is also not a critical issue. The most interesting question, if any, is to look that the dump really does not allow the high energy particles to escape. To study this point we made the shower simulations with the help of the EGS4 program, which have shown that dump absorbs about 97% of the incoming energy. The rest ($\sim$ 3%) comes out mainly in the form of low energy photons.

Figure 12 shows an example of the shower development in the copper dump, and figure 13 shows the distribution of escaped photons.

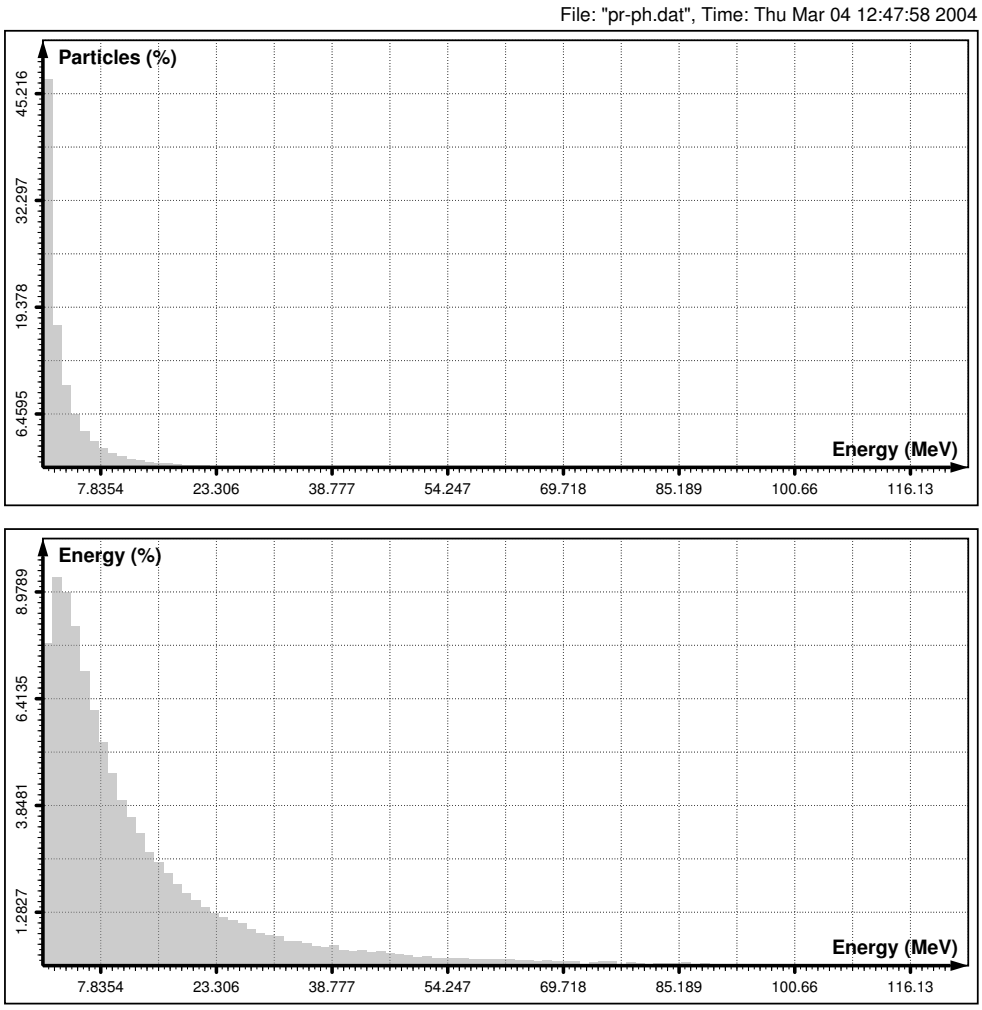

Figure 13: Particle and energy distribution of escaped photons.

5 Conclusion

The main results of this study are summarized in figure 14, where the maximal recommended number of bunches per train is shown as a functions of the rms beam spot area. We propose, that initially one will obtain the information about the beam spot area in a single bunch operation, and only then, having the estimation of maximal number of bunches per train, one will switch to multibunch mode.

The curve in figure 14 is plotted for the bunch charge of 1 nC. Having another bunch charge, let say n nC, one has to divide the number extracted from this figure by n.

Let us remind that for small beam spot areas the main limitations come from the stress limit (figure 11) and for large spots the number of bunches is restricted by the desire to keep the window temperature below $80^\circ - 100^\circ C$ (figure 8).

Note that the marks in figure 14 corresponding to different operational modes were plotted using discussed above theoretical beta functions, the normalized emittance for both planes of $1.5\,mm \cdot mrad$, the energy of 130 MeV, and the bunch charge of 1 nC.

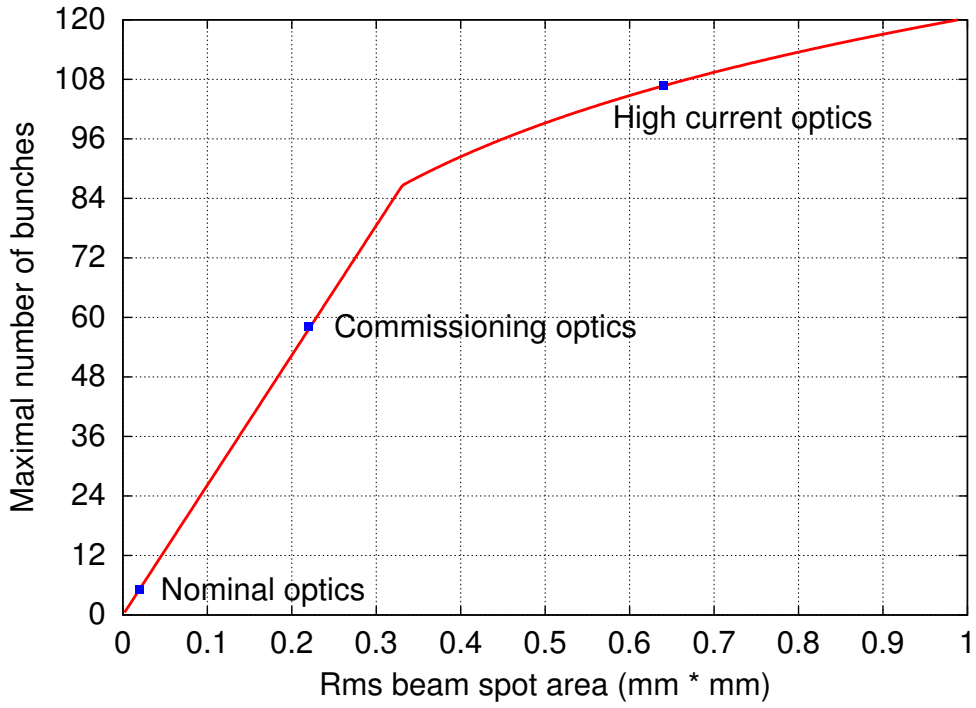

Figure 14: Maximal recommended number of bunches per train as a function of the rms beam spot area. Bunch charge is $1\,nC$. Particle energy is $130\,MeV$.

References

[1] K. Flöttmann. *Commissioning of Injector III.* TESLA Collaboration Meeting, Zeuthen, January 22, 2004.

[2] A. Brenger. *Private communication.*

[3] N. Golubeva. *TTF2 Optics: 28.04.2003.* Unpublished.

[4] E. Schneidmiller. *At z = 13 600 m:* $\beta_{x,y} = 18.8\,m$, $\alpha_{x,y} = -0.42$. Private communication.

[5] H. Schlarb. *Some numbers for high gradient test.* Private communication.

[6] *SASE FEL at the TESLA Facility, Phase 2.* The TESLA Test Facility FEL team. TESLA-FEL-2002-01, 2002.

[7] M. Ferrario, K. Flöttmann, B. Grigoryan, T. Limberg, Ph. Piot. *Conceptual Design of the XFEL Photoinjector.* TESLA-FEL 2001-03, February 2001.

[8] P. Castro. *Monte Carlo Simulations of Emittance measurements at TTF2.* Technical Note 2003-03, September 2003.

[9] P. Castro. *TTF2 optics: a parameter list.* http://www.desy.de/pcastro/TTF2/documents/optics_param.html.

[10] P. Emma, R. Brinkmann. *Emittance Dilution Through Coherent Energy Spread Generation in Bending Systems.* SLAC-PUB-7554, May 1997.

[11] M. Dohlus, A. Kabel, T. Limberg. *Optimal Beam Optics in the TTF-FEL Bunch Compression Sections: Minimizing the Emittance Growth.* Proceedings of the 1999 Particle Accelerator Conference, New York, 1999, pp. 1650-1652.

[12] V. Balandin, K. Flöttmann, N. Golubeva, M. Körfer. *Studies of the Collimator system for the TTF Phase 2.* TESLA 2003-17.

[13] M. Seidel. *An Exit Window for the TESLA Test Facility.* TESLA Report 95-18.

[14] Jan M. Zazula. *From Particle Cascade Simulations (FLUKA) to Finite Element Heat Transfer and Structural Deformation Analysis (ANSYS).* Proc. of the 2-th Workshop on Simulating Accelerator Radiation Environment, CERN, Geneva, October 9-11, 1995.

[15] H. Schlarb. *Collimation System for the VUV Free-Electron Laser at the TESLA Test Facility.* DESY-THESIS-2001-055.

[16] http://www.efunda.com/materials/

[17] R. Brinkmann, A. Drozhdin, D. Schulte, M. Seidel. *The TESLA Beam Collimation System.* TESLA 95-25, December 1995.

[18] W.R. Nelson, H. Hirayma, and D.W.O. Rogers. *The EGS4 code system.* SLAC Report 265 (1985).

[19] V. Balandin. *The ESG4 based programs for the calculations of the energy balance at the passage of particles through material samples of different geometries.*

[20] P. Sievers. *Elastic stress waves in matter due to rapid heating by an intense high-energy particle beam.* LAB.II/BT/74-2, June 1974.